LETTER

doi:10.1038/nature10667

Jamming by shear

Dapeng Bi[1], Jie Zhang[2,3,4], Bulbul Chakraborty[1] & R. P. Behringer[4]

A broad class of disordered materials including foams, glassy molecular systems, colloids and granular materials can form jammed states. A jammed system can resist small stresses without deforming irreversibly, whereas unjammed systems flow under any applied stresses. The broad applicability of the Liu–Nagel jamming concept[1,2] has attracted intensive theoretical and modelling interest but has prompted less experimental effort[1–6]. In the Liu–Nagel framework, jammed states of athermal systems exist only above a certain critical density. Although numerical simulations for particles that do not experience friction broadly support this idea[7–13], the nature of the jamming transition for frictional grains is less clear[14–17]. Here we show that jamming of frictional, disk-shaped grains can be induced by the application of shear stress at densities lower than the critical value, at which isotropic (shear-free) jamming occurs. These jammed states have a much richer phenomenology than the isotropic jammed states: for small applied shear stresses, the states are fragile, with a strong force network that percolates only in one direction. A minimum shear stress is needed to create robust, shear-jammed states with a strong force network percolating in all directions. The transitions from unjammed to fragile states and from fragile to shear-jammed states are controlled by the fraction of force-bearing grains. The fractions at which these transitions occur are statistically independent of the density. Jammed states with densities lower than the critical value have an anisotropic fabric (contact network). The minimum anisotropy of shear-jammed states vanishes as the density approaches the critical value from below, in a manner reminiscent of an order–disorder transition.

Cohesionless granular materials form jammed states only under external stress, as explored extensively in the soil mechanics literature[18]. In the zero-temperature ($T = 0$) plane of the Liu–Nagel jamming diagram[1–3] (Fig. 1a), increased packing fraction (ϕ) induces jamming and positive pressure, and shear stress (τ) induces irreversible flow at the yield stress line (Fig. 1a, black line). Simulations of frictionless grains typically probe jamming near the critical point at $T = 0$, $\tau = 0$ and $\phi = \phi_J$, through isotropic compression or decompression[7–9], or along the yield stress line[11–13,19,20]. The numerical value of ϕ_J depends on the protocol for preparing the jammed states. However, the characteristics of the transition are robust[21]. Only a few experiments[4–6,22] have investigated the Liu–Nagel jamming model[1,2] for physical systems consisting of particles with friction. For example, by using isotropically confined frictional disks it was found[4] that friction only weakly affects certain aspects of jamming, such as the packing fraction ($\phi \approx 0.842$), but that other aspects, such as average number of contacts at jamming, are more strongly dependent on friction, as expected[15].

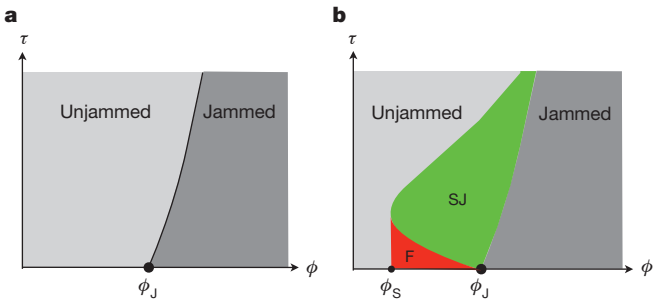

Figure 1 | Jamming phase diagrams in the $T = 0$ plane. **a**, Original Liu–Nagel jamming phase diagram[1]. The boundary between unjammed and jammed regions is the yield stress line. Unjamming can be induced by decreasing the packing fraction or increasing the shear stress. **b**, Generalized jamming diagram including the shear-jammed (SJ) and fragile (F) states. Along the ϕ axis, there are two special densities: ϕ_S, below which there is no shear jamming, and ϕ_J, above which isotropically jammed states exist. For $\phi_S \leq \phi \leq \phi_J$, jamming can occur with application of shear stress.

We report stable static states that jam only under a minimum shear stress. These states are outside the jammed region of Fig. 1a and alter the jamming diagram as illustrated in Fig. 1b. Of special note is the line separating two qualitatively different classes of states: the fragile states and the shear-jammed states. As we show below, this line is the locus of shear stresses marking a percolation transition. Shear-jammed states have not been reported in typical (that is, frictionless) models of jamming, which involve isotropically compressed particles and where additional relaxation may be induced to find a lower-energy state[7,15]. Our systems differ from these models in several key aspects: they consist of frictional (photoelastic) disks (Supplementary Fig. 1) prepared at densities below (and above) ϕ_J; they are subjected to pure (volume-preserving) shear applied in small strain steps, allowing the system spontaneously to relax between steps; and they rest on a weakly frictional substrate, with forces that are an order of magnitude smaller than typical interparticle forces at jamming. We obtained stress data, that is, values of τ, pressure (P) and the fabric tensor ($\hat{R}$). The eigenvalues, R_1 and R_2, of $\hat{R}$ yield the mean contact number, $Z = R_1 + R_2$, and a measure of contact anisotropy, $\rho = R_2 - R_1$. In addition, we analysed the spatial organization of contact forces. Experimental details can be found in Methods.

Ascertaining that states are macroscopically jammed is non-trivial. Necessary requirements are non-zero P and τ and the ability to resist any small incremental stress. For frictionless grains, these conditions are met if Z exceeds Z_{iso} (refs 7, 11), where the number of mechanical equilibrium constraints equals the number of degrees of freedom. For large N, isotropic jammed states exist for $\phi \geq \phi_J$, where ϕ_J depends only on the spatial dimension for a given protocol[7].

For frictional grains, a minimal parameter set for jamming has not been clearly determined. Although Z is a key parameter for mechanical stability, the minimum number of contacts needed for jamming can span a range of values, depending on friction and preparation[14,15,23]. For the disks used here, a reasonable criterion for isotropic jamming was found to be $Z \geq 3.0$ to ~ 3.1 (ref. 4), for which $\phi_J \approx 0.842$ (Supplementary Fig. 3).

A distinguishing property of granular jammed states is the existence of force networks. To characterize the states obtained by shearing at $\phi < \phi_J$, we consider the contact force and fabric networks, and their correlation with the properties of the stress tensor[24] and the fraction of non-rattler grains, f_{NR} (Supplementary Figs 2 and 4). It is known from earlier studies that force networks in jammed packings of dry grains

[1]Martin Fisher School of Physics, Brandeis University, Waltham, Massachusetts 02454, USA. [2]Institute of Natural Sciences and Department of Physics, Shanghai Jiao Tong University, Shanghai 200240, China. [3]Department of Physics, Indiana University Purdue University Fort Wayne, Fort Wayne, Indiana 46805, USA. [4]Department of Physics, Duke University, Durham, North Carolina 27708, USA.

can be separated into a strong network (in which each contact force magnitude satisfies $f > f_{avg}$, where f_{avg} is the average of all contact force magnitudes over all force-bearing contacts in the system) and a complementary weak network[24,25]. We identify a strong force network with the largest cluster of grains that is connected via contact forces with magnitudes $f > f_{avg}$.

Starting from an unjammed state (Fig. 2), the strong force network undergoes two sequential percolation transitions controlled by the non-rattler fraction, f_{NR} (ref. 26; here we define grains with at least two force-bearing contacts as non-rattler grains). Experimentally, the shear strain controls f_{NR}. Monotonic increases in shear strain generally increase f_{NR} (Supplementary Fig. 5) and tune the system through the percolation transitions. For $f_{NR} < 0.4$, the network of force-bearing grains does not percolate in any direction of the sheared packing. There are small residual values of P and τ for these states due only to experimental noise and the small frictional forces exerted on the grains by the base (Methods). We refer to these states as 'unjammed'. As f_{NR} increases above ~0.7, the strong force network percolates in the compressive direction but not transverse to it. We refer to these states as 'fragile'; they have a strong force network that carries the majority of the shear stress (deviatoric stress) but which spans the system only in the compressive direction. The weak force network, by contrast, acts like a fluid, supporting a less anisotropic stress tensor[24]. We expect that in the limit of infinitely rigid grains, these fragile states would be able to support only loads along the compressive direction without undergoing plastic rearrangement[27]. Because the experimental system is composed of deformable grains, there is a small regime of elastic response in the dilational direction even for the fragile states. At $f_{NR} = 0.83 \pm 0.02$, the strong force network percolates in both directions. These states, which we refer to as 'shear jammed', are characterized by two non-parallel populations of force chains. The classification of shear-jammed, fragile and unjammed states has relied on identifying the $f > kf_{avg}$ (with $k = 1$) cluster as the strong force network (where f refers to the individual contact force magnitude). We show in Supplementary Fig. 6 that this definition is robust with respect to the choice of the threshold (k), and that at $f_{NR} = 0.83$ all k-clusters with $0 \leq k \leq 1.2$ have percolated in the dilational direction. The experiment shown in Supplementary Movie 1 illustrates the evolution of force networks and the percolation events.

The Liu–Nagel jamming diagram needs to be modified to include the fragile and shear-jammed states. Figure 2c shows a τ–ϕ plot of shear-jammed (green), fragile (red) and unjammed (black) states, as distinguished by the natures of their force networks. For each $\phi < \phi_J$, there is a minimum shear stress, $\tau_0(\phi)$, needed to create a shear-jammed state, and $\tau_0 \to 0$ as $\phi \to \phi_J$ from below. As shown in Fig. 2b (see also Supplementary Figs 5 and 6), the pure shear strain imposed in the experiment induces shear jamming by increasing the non-rattler fraction, f_{NR}, which leads to the two percolation transitions. Continued shear pushes the system to the yield stress line (Fig. 2c, purple symbols). For $\phi > \phi_J$, jammed states with a strong force network percolating in all directions occur along the ϕ axis at $\tau = 0$.

The formation of fragile and shear-jammed states depends on the possibility of creating anisotropic contact networks (fabric[24,28,29]; discussed in detail in Supplementary Figs 5, 7 and 8), which form a backbone for the stresses[27]. The anisotropies of the stress tensor and the fabric tensor are intimately related in these states[24,29]. Models, physical particle properties or protocols that preclude the formation of this backbone would not lead to these states.

Theoretical support for shear-jammed states comes from recent simulations[16] that probed systems of frictional grains subject to quasi-static steady shear along the yield stress line and showed a discontinuous transition in the τ–ϕ phase curve from jammed to unjammed states at a value of ϕ that is consistent with our observations for ϕ_S, the lowest value of ϕ for which shear jamming occurs. These simulations correspond to moving along the yield stress line in Fig. 2c (purple) towards lower values of ϕ and arriving at the 'nose' of the jamming curve at ϕ_S.

The relationship between the fabric and stress anisotropies, expressed in Fig. 3a as a plot of ρ versus τ for all sheared states, is analogous to that between magnetization and magnetic field in a magnetic system. As

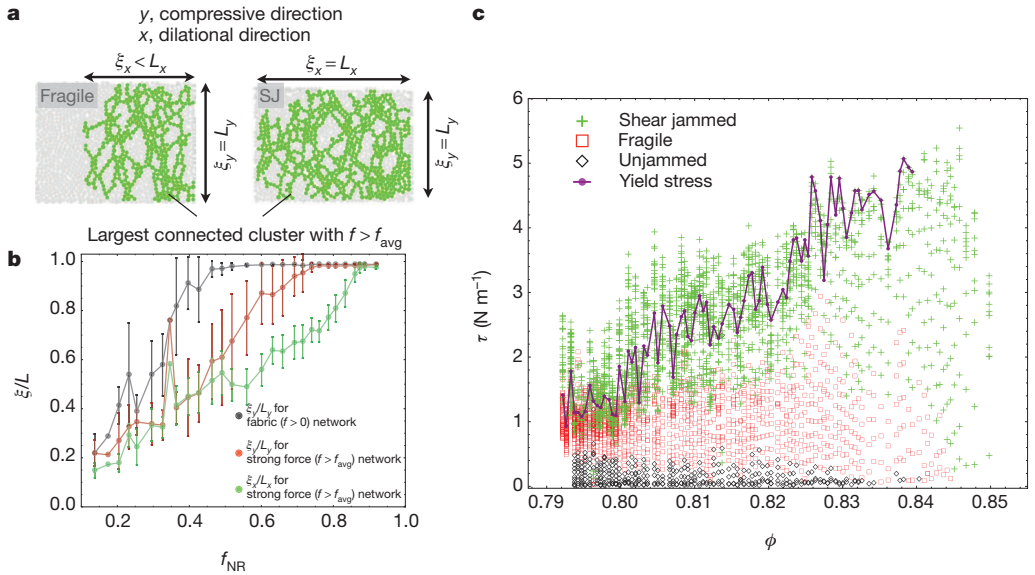

Figure 2 | Using percolation analysis of the strong force network to classify states. **a**, Snapshots of typical fragile and shear-jammed states. Left: fragile states have a strong force network ($f > f_{avg}$) that is percolated in the compressive (y) direction but not the dilational (x) direction. Right: shear-jammed states have a strong force network that is percolated in all directions. ξ_x and ξ_y are the linear sizes associated with the largest connected cluster in the strong force network. L_x and L_y are box dimensions. **b**, Plots of cluster size/box dimension ratio (ξ/L) versus f_{NR} for the fabric and the strong force networks (Supplementary Fig. 6): black, fabric network in the compressive direction; red, strong force network in the compressive direction; green, strong force network in the dilational direction. Data show mean ± s.d. **c**, Scatter plot of states in the τ–ϕ plane. The red, green and black points correspond to fragile (percolation in one direction), shear-jammed (percolation in all directions) and non-percolating networks, respectively, and are defined by the criterion of force network percolation as shown in **b**. The purple line is the yield stress line. For each $\phi < \phi_J$, the yield stress is obtained by averaging over the stress values just before plastic rearrangements occur in the forward shear time trace[11]. For $\phi > \phi_J$, owing to experimental limitations, we do not have enough statistics to calculate the yield stress.

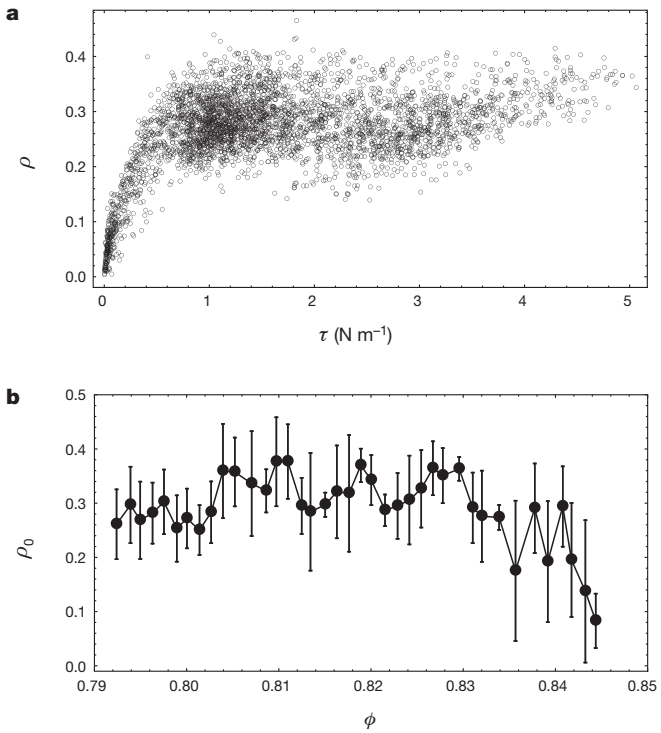

Figure 3 | Relationship between fabric and stress anisotropies and how they vanish at ϕ_J. **a**, Scatter plot of ρ versus τ for all experimental states ($\phi_S \leq \phi \leq \phi_J$) created under shear. Note that $\rho \approx 0.67\tau$ as $\tau \to 0$. **b**, Fabric anisotropy ($\rho_0(\phi)$) for states with $f_{NR} = 0.83$ (along the boundary between fragile (red) and shear-jammed (green) states (Fig. 2c)). This is the lowest fabric anisotropy needed to obtain shear-jammed states. Data show mean ± s.d.

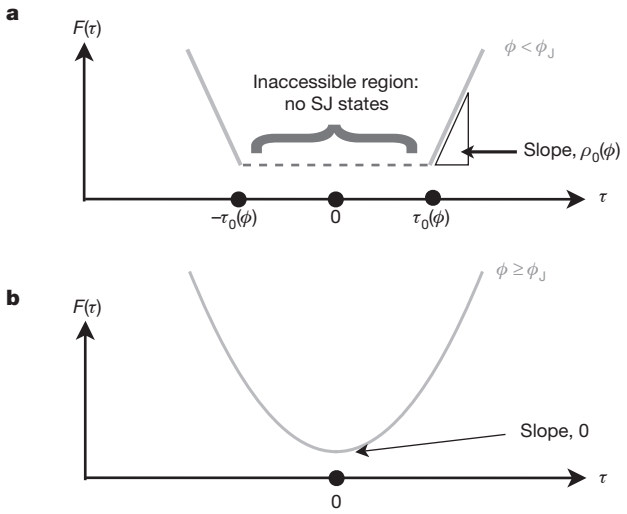

Figure 4 | Effective free energy for shear-jammed states. The panels show the τ-dependent part of the effective free energy ($F(\tau)$) for different ranges of ϕ. **a**, For $\phi < \phi_J$, there is an excluded region, $-\tau_0 < \tau < \tau_0$, where fragile states exist but shear-jammed states do not. The points at which the curve intersects this excluded region correspond to $\pm\tau_0(\phi)$, and the slopes at these points determine $\rho_0(\phi)$. **b**, For $\phi \geq \phi_J$, there is no excluded region, all values of τ are allowed and $\rho_0 = 0$.

shown in Supplementary Figs 7–9, under cyclic shear the ρ–τ relationship is essentially hysteresis free whereas the stress–strain relationship has large hysteresis loops. Along $\tau = \tau_0(\phi)$, that is, at the onset of shear jamming, the fabric anisotropy ($\rho_0(\phi)$) is roughly independent of ϕ for values of ϕ much less than ϕ_J, but vanishes at $\phi = \phi_J$ and stays zero for $\phi > \phi_J$ (Fig. 3b). This suggests that ρ_0 acts as an order parameter for the shear-jammed states (it is non-zero for such states and zero for isotropic jammed states) and that ϕ_J marks an order–disorder transition at which jammed states become isotropic. For a magnet, the order parameter is the zero-field magnetization, whereas the order parameter for the shear-jammed states, ρ_0, is measured along the $\tau_0(\phi)$ line, the lower limit for jammed states to exist. For systems in thermal equilibrium, derivatives of the free energy define relationships between an order parameter and the conjugate external field. In analogy, we define an 'effective free energy' (F) through the relationship $\rho = \partial F/\partial\tau$. The results for $\rho_0(\phi)$ and $\tau_0(\phi)$ suggest an empirical form for F that is illustrated in Fig. 4. This form is consistent with the ρ–τ relationship for cyclically sheared states (Supplementary Figs 7–9). For $\phi_S < \phi < \phi_J$, there is an excluded region, $-\tau_0 < \tau < \tau_0$, with fragile but not shear-jammed states, and the slope of F (as a function of τ) at the boundary of this regime is ρ_0. As $\phi \to \phi_J$ from below, the excluded region vanishes and $\rho_0 \to 0$. Ideally, such an effective free energy would be related to the probability density of shear-jammed states at given values of ϕ and τ, which could be obtained from simulations of sheared frictional grains.

The present jamming diagram, deduced from physical experiments with frictional particles, differs substantially from the jamming diagram based on simulations of frictionless particles. We observe new classes of states that exist only under shear, have anisotropic force and fabric networks, and have an order parameter that vanishes as ϕ increases beyond a threshold comparable to ϕ_J for isotropic jammed states. The fraction of non-rattler grains (f_{NR}) controls the percolation of the force networks and emerges as the single parameter distinguishing between unjammed, fragile and shear-jammed states. The shear-jammed states occupy a large region of parameter space and are important in determining the response of frictional granular materials to external stresses. The yield stress of shear-jammed states vanishes discontinuously at $\phi_S < \phi_J$ (ref. 16). The origin of these states is probably related to dilatancy, that is, the tendency of dense granular matter, under constant pressure, to expand under shear. Under constant-area conditions such as in the experiments studied here, shearing leads to jamming[17,27]. Our systems are quasi-two-dimensional and an important question for further study is what happens in fully three-dimensional systems.

METHODS SUMMARY

We applied pure shear strain to a system of 1,568 frictional, bidisperse, photoelastic disks contained in a biaxial device[4,22,30]. This device can deform the system, keeping the area (A) and ϕ fixed, to perform isotropic compression or pure shear. In many soil mechanics approaches, biaxial deformations are achieved by compressing in one direction while keeping the normal stress constant in the remaining direction[18,29]. Using photoelastic particles, we determine the location of, and forces (f) at, interparticle contacts[30], and from these construct the stress tensor ($\hat{\sigma}$) and a contact fabric tensor[24,29] ($\hat{R}$):

$$\hat{\sigma} = \frac{1}{V}\sum_{i\neq j} \mathbf{r}_{ij} \otimes \mathbf{f}_{ij}$$

$$\hat{R} = \frac{1}{N}\sum_{i\neq j} \frac{\mathbf{r}_{ij}}{\|\mathbf{r}_{ij}\|} \otimes \frac{\mathbf{r}_{ij}}{\|\mathbf{r}_{ij}\|}$$

Here $\mathbf{r}_{ij}$ is the contact vector from the centre of grain i to the interparticle contact between grains i and j, $\mathbf{f}_{ij}$ is the force vector associated with this contact and '$\otimes$' denotes a vector outer product. Also, V is the volume of the system (or area in two dimensions) and N is the number of non-rattler particles (particles with at least two contacts[4,22]). Denoting the principal stresses by σ_1 and σ_2, the pressure is given by $P = (\sigma_1 + \sigma_2)/2$ and the shear stress is given by $\tau = (\sigma_2 - \sigma_1)/2$. Denoting the eigenvalues of $\hat{R}$ by R_1 and R_2, the mean contact number per particle is $Z = R_1 + R_2$ and $\rho = R_2 - R_1$ or ρ/Z characterizes the contact network anisotropy.

The experiments span $\phi_S \leq \phi \leq \phi_L$, where $\phi_S = 0.792$ and $\phi_L = 0.850$. For each value of ϕ, the walls of the biaxial device were initially configured in a square, with the particles in nominally random positions. For $\phi < \phi_J \approx 0.842$, the initial isotropic state was unjammed. For $\phi > \phi_J$, we initialized the system by tapping gently to relax the stresses to their lowest value. For all ϕ, after initializing the system we subsequently made small quasi-static pure shear steps, allowing the system spontaneously to relax for at least several minutes between steps. The typical strain step was of size $\delta\varepsilon \approx 0.003$. For sufficient shear, the system achieved a manifestly

jammed state, with a network of force chains (Supplementary Fig. 1) provided that $\phi > \phi_S$. We also carried out some cyclic shear experiments[22] (Supplementary Figs 7–9). These experiments involved six cycles, each consisting of a forward and a reverse shear strain, and the data from these cycles provide valuable information about the evolution of the relevant networks.

Received 14 March; accepted 25 October 2011.

1. Liu, A. & Nagel, S. Jamming is not just cool any more. *Nature* **396,** 21–22 (1998).
2. Liu, A. J. & Nagel, S. R. Granular and jammed materials. *Soft Matter* **6,** 2869–2870 (2010).
3. Trappe, V., Prasad, V., Cipelletti, L., Segre, P. N. & Weitz, D. A. Jamming phase diagram for attractive particles. *Nature* **411,** 772–775 (2001).
4. Majmudar, T. S., Sperl, M., Luding, S. & Behringer, R. P. Jamming transition in granular systems. *Phys. Rev. Lett.* **98,** 058001 (2007).
5. Lechenault, F. *et al.* Critical scaling and heterogeneous superdiffusion across the jamming/rigidity transition of a granular glass. *Europhys. Lett.* **83,** 46003 (2008).
6. Candelier, R. & Dauchot, O. Creep motion of an intruder within a granular glass close to jamming. *Phys. Rev. Lett.* **103,** 128001 (2009).
7. O'Hern, C. S., Silbert, L. E., Liu, A. J. & Nagel, S. R. Jamming at zero temperature and zero applied stress: the epitome of disorder. *Phys. Rev. E* **68,** 011306 (2003).
8. Silbert, L. E., Liu, A. J. & Nagel, S. R. Structural signatures of the unjamming transition at zero temperature. *Phys. Rev. E* **73,** 041304 (2006).
9. Silbert, L. E., Liu, A. J. & Nagel, S. R. Vibrations and diverging length scales near the unjamming transition. *Phys. Rev. Lett.* **95,** 098301 (2005).
10. Wyart, M. On the rigidity of amorphous solids. *Ann. Phys. Fr.* **30,** 1–96 (2005).
11. Heussinger, C. & Barrat, J.-L. Jamming transition as probed by quasistatic shear flow. *Phys. Rev. Lett.* **102,** 218303 (2009).
12. Olsson, P. & Teitel, S. Critical scaling of shear viscosity at the jamming transition. *Phys. Rev. Lett.* **99,** 178001 (2007).
13. Olsson, P. & Teitel, S. Glassiness, rigidity and jamming of frictionless soft core disks. *Phys. Rev. E* **83,** 031307 (2011).
14. Makse, H., Johnson, D. L. & Schwartz, L. M. Packing of compressible granular materials. *Phys. Rev. Lett.* **84,** 4160–4163 (2000).
15. Silbert, L. E. Jamming of frictional spheres and random loose packing. *Soft Matter* **6,** 2918–2924 (2010).
16. Otsuki, M. & Hayakawa, H. Critical scaling near jamming transition for frictional granular particles. *Phys. Rev. E* **83,** 051301 (2011).
17. Pastore, M., Ciamarra, M. P. & Coniglio, A. Flow and jam of frictional athermal systems under shear stress. *Phil. Mag.* **91,** 2006–2013 (2011).
18. Nedderman, R. M. *Statics and Kinematics of Granular Materials* (Cambridge Univ. Press, 1992).
19. Hatano, T. Scaling properties of granular rheology near the jamming transition. *J. Phys. Soc. Jpn* **77,** 123002 (2008).
20. Peyneau, P.-E. & Roux, J.-N. Frictionless bead packs have macroscopic friction, but no dilatancy. *Phys. Rev. E* **78,** 011307 (2008).
21. Ciamarra, M. P. Nicodemi, M. & Coniglio, A. Recent results on the jamming phase diagram. *Soft Matter* **6,** 2871–2874 (2010).
22. Zhang, J., Majmudar, T. S., Tordesillas, A. & Behringer, R. P. Statistical properties of a 2D granular material subjected to cyclic shear. *Granul. Matter* **12,** 159–172 (2010).
23. Henkes, S., van Hecke, M. & van Saarloos, W. Critical jamming of frictional grains in the generalized isostaticity picture. *Europhys. Lett.* **90,** 14003 (2010).
24. Radjai, F., Wolf, D. E., Jean, M. & Moreau, J.-J. Bimodal character of stress transmission in granular packings. *Phys. Rev. Lett.* **80,** 61–64 (1998).
25. Walker, D. M. *et al.* Percolating contact subnetworks on the edge of isostaticity. *Granul. Matter* **13,** 233–240 (2011).
26. Göncü, F., Duran, O. & Luding, S. Constitutive relations for the isotropic deformation of frictionless packings of polydisperse spheres. *C.R. Méc.* **338,** 570–586 (2010).
27. Cates, M. E., Wittmer, J. P., Bouchaud, J.-P. & Claudin, P. Jamming, force chains, and fragile matter. *Phys. Rev. Lett.* **81,** 1841–1844 (1998).
28. Goddard, J. D. *Continuum Modeling of Granular Assemblies* 1–24 (Kluwer, 1998).
29. Alonso-Marroquín, F., Luding, S., Herrmann, H. J. & Vardoulakis, I. Role of anisotropy in the elastoplastic response of a polygonal packing. *Phys. Rev. E* **71,** 051304 (2005).
30. Majmudar, T. S. & Behringer, R. P. Contact force measurements and stress-induced anisotropy in granular materials. *Nature* **435,** 1079–1082 (2005).

Supplementary Information is linked to the online version of the paper at www.nature.com/nature.

Acknowledgements D.B. and B.C. acknowledge support from US NSF grant DMR-0905880. R.P.B. and J.Z. acknowledge support from US NSF grants DMR-0906908 and NSF-0835571, and from US ARO grant W911NF-07-1-1031. B.C. and R.P.B. acknowledge the hospitality of the Aspen Center for Physics and discussions with S. Teitel, H. Hayakawa and M. Otsuki. D.B. and B.C. acknowledge discussions with M. Mailman.

Author Contributions All authors contributed in comparably equal ways. Specifically, R.P.B. and J.Z. designed the experimental project, including the force-inverse algorithm, and performed the experiments. B.C. and D.B. performed the theoretical analysis. D.B. and J.Z. carried out the data analysis. All authors contributed equally to writing the manuscript.

Author Information Reprints and permissions information is available at www.nature.com/reprints. The authors declare no competing financial interests. Readers are welcome to comment on the online version of this article at www.nature.com/nature. Correspondence and requests for materials should be addressed to R.P.B. (bob@phy.duke.edu).